

Masked Diffusion Modeling for Anomaly Detection

Lixing Zhang¹ Yuchen Liang² Liyan Xie¹
¹University of Minnesota ²Ohio State University

🔗 Code: <https://github.com/lxzhang1/MaskDiff-AD>

Abstract

Anomaly detection aims to identify samples that deviate from the nominal data distribution and is central to many safety-critical applications. However, developing effective anomaly detection methods for categorical, mixed-type, and discrete sequence data remains challenging and relatively underexplored. Masked diffusion models provide a natural way to model such data by learning to recover masked values from the remaining visible context. In this paper, we propose *Masked Diffusion for Anomaly Detection* (MaskDiff-AD), a forward-only method based on masked diffusion models trained only on nominal data. Given a test sample, MaskDiff-AD constructs anomaly scores from the difficulty of reconstructing randomly masked coordinates, yielding a content-sensitive score that operates directly on discrete state spaces while avoiding reverse-time sampling. We also develop a non-parametric variant of MaskDiff-AD and provide theoretical guarantees by characterizing Type-I and Type-II errors under a fixed detection threshold. Experiments on fourteen categorical and mixed-type tabular datasets from ADBench and UADAD, as well as four text anomaly detection datasets from NLP-ADBench, show that MaskDiff-AD achieves competitive performance against classical, diffusion-based, and recent tabular/text anomaly detection baselines. Notably, MaskDiff-AD achieves the best overall average rank, outperforming all twelve tabular baseline methods.

1 Introduction

Anomaly detection aims to identify observations that deviate significantly from the majority of the data (i.e., the data-generating distribution) [1, 2, 3]. As a core problem in machine learning and statistics, it has been studied for decades and plays an important role in a wide range of applications, including healthcare [4, 5], finance [6], cybersecurity [6], manufacturing [7], particle physics [8], and geospatial analysis [9]. Despite this long history, the increasing prevalence of large-scale datasets with discrete or mixed data types has exposed important limitations of many classical methods [10]. Many modern anomaly detection problems involve categorical, discrete, or mixed-type data, including tabular records with categorical attributes, transaction and claims data with heterogeneous feature types, and tokenized text sequences [11, 12]. These data types are not naturally suited to methods built around Euclidean geometry or continuous densities. These challenges motivate the development of anomaly detection methods that are well-suited to the structural characteristics of discrete-type data, while being scalable, interpretable, and sufficiently expressive.

Recently, diffusion models have provided a flexible framework for learning complex data distributions [13, 14]. Among them, discrete diffusion models, especially masked diffusion models, have further extended this capability to discrete domains such as text, music, and molecular data [15, 16]. Notably, on certain tasks, masked diffusion models have demonstrated superior performance compared to autoregressive approaches [17, 18]. However, as with other generative models, the

Main contact: liyanxie@umn.edu

majority of research on diffusion models has focused on improving sampling efficiency and enabling controllable generation (e.g., [17, 19, 20]). In contrast, relatively few studies have explored their use, particularly that of masked diffusion models, for anomaly detection.

In the literature, one notable work has explored the use of (continuous) diffusion models for anomaly detection: the Diffusion Time Estimation (DTE) framework [21]. This approach estimates the posterior distribution over the diffusion time and uses the inferred corruption level as an anomaly score, thereby avoiding the need for expensive reverse-time sampling. However, a key component of this framework relies on the Gaussian corruption structure, with a possible discrete analogue in uniform discrete diffusion models. As we show in Section 3, this approach does not readily extend to masked diffusion models. In particular, due to the absorbing masking mechanism, the DTE-style posterior becomes ill-posed: it either collapses to identical values across all clean categorical samples or depends solely on the masking pattern of the corrupted observation, rather than the underlying distribution of the test data.

Masked diffusion models (MDM) have recently gained increasing attention for modeling discrete data [15]. They learn to reconstruct clean categorical values from partially masked observations, such as learning to predict masked tokens from the remaining context. Motivated by the masking procedure, we propose *Masked Diffusion for Anomaly Detection* (MaskDiff-AD). The key idea is to employ a *mask-corruption level* tailored to the masked discrete diffusion process, and to use the corresponding *single-step reconstruction difficulty* as the anomaly score. In other words, instead of asking at which corruption time a test sample becomes indistinguishable from noisy normal data, MaskDiff-AD asks how difficult it is to reconstruct masked coordinates from the remaining visible context under a model trained only on normal data. A normal sample should have coordinates that are mutually consistent and therefore easy to predict from one another, whereas an anomalous sample should induce larger masked reconstruction surprisal. This yields a content-sensitive anomaly score without reverse-time sampling or iterative imputation.

The contributions of our work are summarized as follows:

- We formulate anomaly detection on discrete state spaces using masked diffusion models and show why a direct DTE-style time posterior degenerates in this setting.
- We introduce MaskDiff-AD, a masked reconstruction-based anomaly detection method that is trained *only on nominal samples*, computationally efficient, and does not require reverse-time sampling. We also develop both non-parametric and parametric implementations of MaskDiff-AD.
- We provide theoretical analysis for the proposed reconstruction score, including guarantees on Type-I and Type-II errors.
- We demonstrate the effectiveness of our MaskDiff-AD with extensive experiments on categorical tabular, mixed-type tabular, and text anomaly detection benchmarks.

Related Work. Our work is connected to several lines of research. Classical anomaly detection methods include distance-based approaches such as k -nearest neighbors [22], tree-based methods such as Isolation Forest [23], and distributional or copula-based scores such as ECOD [24] and COPOD [25]. These methods are often efficient and broadly applicable, but their performance can depend strongly on the chosen representation or distance, especially for categorical and mixed-type data [10, 26]. Recent tabular anomaly detection methods seek to capture richer feature dependencies, including masked cell modeling (MCM) [27], non-parametric transformers for anomaly detection (NPT-AD) [28], internal contrastive learning (ICL) [29], CompreX [30], and decomposed

representation learning [31]. Our method shares the goal of modeling feature dependencies, but does so through the forward masking and conditional reconstruction structure of absorbing discrete diffusion.

Generative models for anomaly detection have been extensively studied, especially for image data. Representative examples include autoencoder and variational-autoencoder based detectors [32, 33], hybrid autoencoding-density models such as DAGMM [34], GAN-based detectors such as AnoGAN and GANomaly [35, 36], and flow-based visual detectors such as DifferNet [37].

Diffusion models have also recently been explored for anomaly detection through reconstruction-based, density-based, and hybrid scoring mechanisms [38]. Representative diffusion-based anomaly detection methods include medical and visual reconstruction methods such as AnoDDPM [39], DDAD [40], and DiffusionAD [41]. These methods are primarily developed for continuous data domains, especially for (medical) image data, where anomaly scores are often derived from denoising error, likelihood surrogates, or reconstruction discrepancy after reverse diffusion.

Diffusion time estimation (DTE) [21] is a recent method for anomaly detection and is efficient because it replaces expensive iterative reverse-chain sampling with a single posterior evaluation, yet retains strong empirical performance on benchmarks. However, its construction relies on the geometry of Gaussian corruption and does not remain discriminative under absorbing masked corruption. Our work instead adapts the diffusion perspective to discrete data by replacing time-posterior estimation with masked reconstruction difficulty. This keeps the computational advantage of forward-only scoring while producing a content-sensitive anomaly signal on the original discrete state space.

2 Preliminaries

We consider anomaly detection over a general discrete state space $\mathcal{X} = \mathcal{X}_1 \times \dots \times \mathcal{X}_d$ and denote each data point as a vector $\mathbf{x} = (x_1, \dots, x_d) \in \mathcal{X}$, where each coordinate $x_j \in \mathcal{X}_j$ takes values in a finite (and potentially different) state space. The goal is to distinguish samples generated from a nominal data-generating distribution from anomalous samples that deviate from this distribution. We denote the nominal distribution by q_0 and assume that the training data consist *only* of normal samples $\mathcal{D}_{\text{tr}} = \{\mathbf{x}_i\}_{i=1}^n$ that are independently and identically sampled from q_0 . At test time, a sample may either follow the same nominal distribution or arise from an unknown anomalous distribution q' that differs significantly from q_0 . The anomalous distribution is not specified during training and no labeled anomalous examples are assumed to be available for training.

Given a test sample $\mathbf{x} \in \mathcal{X}$, an anomaly score is assigned such that a larger score indicates that \mathbf{x} is less likely to have been generated from the normal regime. Formally, we define an anomaly detector as a scoring function $S : \mathcal{X} \rightarrow \mathbb{R}$ and declare a test sample \mathbf{x} to be anomalous if $S(\mathbf{x}) > \gamma$, where γ is the detection threshold chosen by controlling the false alarm rate. One example is to choose γ by requiring $\mathbb{P}_{\mathbf{x} \sim q_0}(S(\mathbf{x}) > \gamma) \leq \alpha$ for a prescribed significance level α . Since the anomalous distribution is unknown, the main challenge is to construct such a score function that is sensitive to distributional deviations while relying only on normal training data.

2.1 Masked Diffusion Models

Masked diffusion models (MDM) provide a generative framework for modeling discrete data by learning to reconstruct clean samples from randomly masked observations at each generation step [15]. Trained on nominal data, MDMs can be viewed as learning the underlying distributional characteristics of the nominal distribution q_0 . As the name suggests, MDMs introduce a special

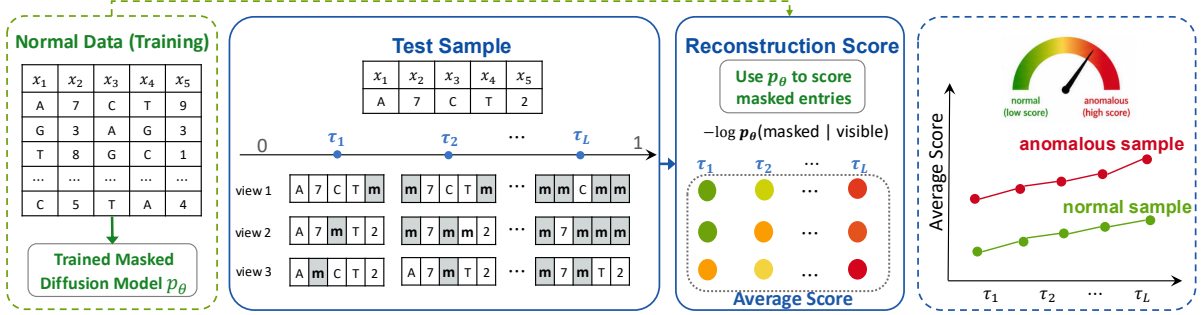


Figure 1: Overview of MaskDiff-AD. We first generate masked probe views of a test sample at multiple levels τ_1, \dots, τ_L , and score each view by the reconstruction surprisal of the masked entries using a trained MDM p_θ on normal-only data. The final anomaly score averages these scores across views and mask levels; larger score values indicate stronger anomaly evidence.

mask state \mathbf{m} that does not belong to any \mathcal{X}_j , resulting in the augmented space:

$$\tilde{\mathcal{X}} := \tilde{\mathcal{X}}_1 \times \dots \times \tilde{\mathcal{X}}_d, \quad \text{with } \tilde{\mathcal{X}}_j := \mathcal{X}_j \cup \{\mathbf{m}\}.$$

MDMs include a forward and a reverse process. Given a clean nominal sample $\mathbf{x}_0 \sim q_0$, the forward process constructs a family of intermediate random variables $\{\mathbf{x}_t\}_{t \in [0,1]}$ that interpolate between clean data \mathbf{x}_0 and the fully masked state $\mathbf{x}_1 = \{\mathbf{m}, \dots, \mathbf{m}\}$. This is implemented as a *masking (a.k.a., absorbing-state) process* with increasing probability to mask over time. Specifically, let $\alpha_t \in [0, 1]$ be a monotone decreasing function with $\alpha_0 \approx 1$ and $\alpha_1 = 0$. With the standard setup in [15, 16, 42], one can show that the conditional forward distribution is

$$q(\mathbf{x}_t | \mathbf{x}_0) = \prod_{j=1}^d \text{Cat}(x_{t,j}; \alpha_t \delta_{x_{0,j}} + (1 - \alpha_t) \delta_{\mathbf{m}}), \quad (1)$$

where $\delta_{x_{0,j}}$ is a delta function centered at $x_{0,j}$. Moreover, once a coordinate becomes masked, it remains masked for all later times, reflecting the absorbing property.

Then, one way to define the reverse process is to model $q_{s|t,0}(\mathbf{x}_s | \mathbf{x}_t, \mu_\theta(\mathbf{x}_t, t))$ for $s < t$. Here $\mu_\theta^j(\mathbf{x}_t, t) := p_\theta^j(\cdot | \mathbf{x}_t)$ is a distribution over \mathcal{X}_j and is intended to approximate the conditional law of the clean coordinate $x_{0,j}$ given the masked view \mathbf{x}_t . To train p_θ^j , one can employ the standard masked diffusion training objective, which is a weighted masked reconstruction loss, as follows:

$$\mathcal{L}_{\text{MDM}}(\theta) = \int_0^1 \mathbb{E}_{\mathbf{x}_0 \sim q_0, \mathbf{x}_t \sim q_{t|0}(\cdot | \mathbf{x}_0)} \left(\sum_{j: x_{t,j} = \mathbf{m}} w(t) \log p_\theta^j(x_{0,j} | \mathbf{x}_t) \right) dt, \quad (2)$$

where $w(t) := \alpha'_t / (1 - \alpha_t)$ is a function of α_t . Essentially, the objective learns to reconstruct the clean data from the partially masked state. After training on nominal data, the learned $p_\theta^j(\cdot | \mathbf{x}_t)$ captures the data distribution of the normal regime. Intuitively, a test sample should be considered normal if its coordinates are predictable from the remaining coordinates under the learned normal-data conditionals. This observation motivates using masked reconstruction or conditional likelihood quantities derived from the masked diffusion model as anomaly scores in the next Section.

3 Methodology

3.1 MaskDiff-AD: Masked Diffusion for Anomaly Detection

Our proposed method consists of two steps. (i) *Probe masking*: given a test sample \mathbf{x} , we generate independent masked views $\tilde{\mathbf{x}}^{(\ell,k)} \sim q_{\tau_\ell}(\cdot | \mathbf{x})$ at multiple masking levels τ_1, \dots, τ_L . (ii) *Reconstruction scoring*: for each masked view, we use the trained masked diffusion model p_θ to compute the reconstruction surprisal of the masked values, and then average these scores across all views and masking levels. The framework is illustrated in Figure 1, and we detail these two steps below.

Probe masking. Let $0 < \tau_1 < \tau_2 < \dots < \tau_L < 1$ be a pre-specified probe grid. At each probe level τ_ℓ , each coordinate of the test sample $\mathbf{x} \in \mathcal{X}$ is replaced by the mask \mathbf{m} independently with the mask probability $1 - \alpha_{\tau_\ell}$ as shown in Eq. (1). This induces the following distribution of the masked view $\tilde{\mathbf{x}}$ under level τ_ℓ :

$$q_{\tau_\ell}(\tilde{\mathbf{x}} | \mathbf{x}) := \prod_{j=1}^d [(1 - \alpha_{\tau_\ell})\mathbf{1}\{\tilde{x}_j = \mathbf{m}\} + \alpha_{\tau_\ell}\mathbf{1}\{\tilde{x}_j = x_j\}], \quad (3)$$

which can be viewed as the special case of Eq. (1) under time $t = \tau_\ell$. For a masked view $\tilde{\mathbf{x}}$, we write $M(\tilde{\mathbf{x}}) := \{j : \tilde{x}_j = \mathbf{m}\}$ and $V(\tilde{\mathbf{x}}) := \{j : \tilde{x}_j \neq \mathbf{m}\}$ for the masked and visible coordinate sets.

Given a chosen integer K , we generate K independent probe-masked views $\tilde{\mathbf{x}}^{(\ell,1)}, \dots, \tilde{\mathbf{x}}^{(\ell,K)}$ for each probe level τ_ℓ :

$$\tilde{\mathbf{x}}^{(\ell,1)}, \dots, \tilde{\mathbf{x}}^{(\ell,K)} \stackrel{iid}{\sim} q_{\tau_\ell}(\cdot | \mathbf{x}), \text{ for } \ell = 1, 2, \dots, L. \quad (4)$$

Larger values of τ_ℓ on average remove more information from the clean sample and therefore produce more heavily corrupted probe views. It is worthwhile noting that the probe levels τ_1, \dots, τ_L and the number of views K are hyperparameters that can be tuned for detection performance. In this work, we use a fixed, uniform probe grid in the main experiments for simplicity. We also perform a sensitivity analysis on probe levels in our numerical experiments.

Reconstruction scoring. We propose to compute the anomaly score by evaluating *how difficult it is to recover the masked coordinates* of a test point under the predictive model trained on nominal data. Formally, denote the masked diffusion model trained from Eq. (2) as $p_\theta^j(\cdot | \tilde{\mathbf{x}})$, *i.e.*, the estimated conditional distribution of the j -th coordinate of the clean data. Then we define the single-probe reconstruction score as

$$s_{\text{rec}}(\mathbf{x}; \tilde{\mathbf{x}}) := -\frac{1}{|M(\tilde{\mathbf{x}})| \vee 1} \sum_{j \in M(\tilde{\mathbf{x}})} \log p_\theta^j(x_j | \tilde{\mathbf{x}}), \quad (5)$$

i.e., the average surprisal of the true values at masked positions. Intuitively, a normal sample should have a lower reconstruction score, because its coordinates are consistent with the dependency structure learned from normal data and are therefore easier to predict from the visible context. In contrast, an anomalous sample is more likely to violate this dependency structure, making its masked coordinates harder to reconstruct and leading to a higher score, as visualized in Figure 1 and confirmed by the toy synthetic example in Figure 2.

To reduce sensitivity to a particular probe level or random mask, and to improve robustness across various anomalous scenarios, we average the reconstruction score in Eq. (5) over L probe levels and K independent masked views per level. Specifically, let $\{\tilde{\mathbf{x}}^{(\ell,k)}\}_{\ell \in [L], k \in [K]}$ be sampled as in Eq. (4), the final aggregated anomaly score is

$$S_{\text{rec}}(\mathbf{x}) := \frac{1}{LK} \sum_{\ell=1}^L \sum_{k=1}^K s_{\text{rec}}(\mathbf{x}; \tilde{\mathbf{x}}^{(\ell,k)}). \quad (6)$$

Algorithm 1 Test-Time MaskDiff-AD

Input: Test sample \mathbf{x} ; pre-trained masked diffusion model $p_{\hat{\theta}}^j(\cdot | \mathbf{x}_t)$ for $j = 1, \dots, d$; probe grids $\{\tau_{\ell}\}_{\ell=1}^L$; number of views per mask level K ; detection threshold γ .

Output: Anomaly label $\hat{y}(\mathbf{x}) \in \{0, 1\}$, where 1 indicates anomalous and 0 indicates normal.

- 1: **for** each $\ell = 1, \dots, L$ and $k = 1, \dots, K$ **do**
 - 2: Sample the corresponding probe-masked view $\tilde{\mathbf{x}}^{(k,\ell)} \sim q_{\tau_{\ell}}(\cdot | \mathbf{x})$ according to Eq. (3).
 - 3: Compute per-view reconstruction difficulty $s_{\text{rec}}^{(k,\ell)}$ according to Eq. (5).
 - 4: **end for**
 - 5: Compute the aggregated anomaly score $S_{\text{rec}}(\mathbf{x})$ according to Eq. (6).
 - 6: **return** Anomaly label $\hat{y}(\mathbf{x}) = \mathbf{1}\{S_{\text{rec}}(\mathbf{x}) > \gamma\}$.
-

Anomaly detection is then performed by comparing $S_{\text{rec}}(\mathbf{x})$ with a pre-specified threshold, where test data with larger scores are classified as anomalous. We refer to the resulting method as *Masked Diffusion for Anomaly Detection* (MaskDiff-AD). The full algorithm is summarized in Algorithm 1.

Remark 1 (Comparison with DTE [21]). *Our work is inspired by the diffusion time estimation (DTE) for anomaly detection [21], which computes the posterior of the diffusion time given the test sample and uses the posterior mean as the anomaly score. We would like to emphasize that DTE does not transfer naturally to MDM here. A natural attempt to extend DTE to MDM is to retain its corruption-time posterior, $q(t | \mathbf{x}) \propto q(t)q_t(\mathbf{x})$. In masked diffusion, however, q_t is defined on the extended space $\tilde{\mathcal{X}}$ that includes the mask token \mathbf{m} . If a clean sample $\mathbf{x} \in \mathcal{X}$ is viewed as an all-visible element of this space, then $q_t(\mathbf{x}) = \alpha_t^d q_0(\mathbf{x})$, so the resulting posterior $q(t | \mathbf{x}) \propto q(t)\alpha_t^d$ is identical for every clean test sample and therefore contains no discriminative signal. This motivated us to propose the reconstruction-based anomaly score instead under MDM.*

3.2 Some Variants of the Proposed Method

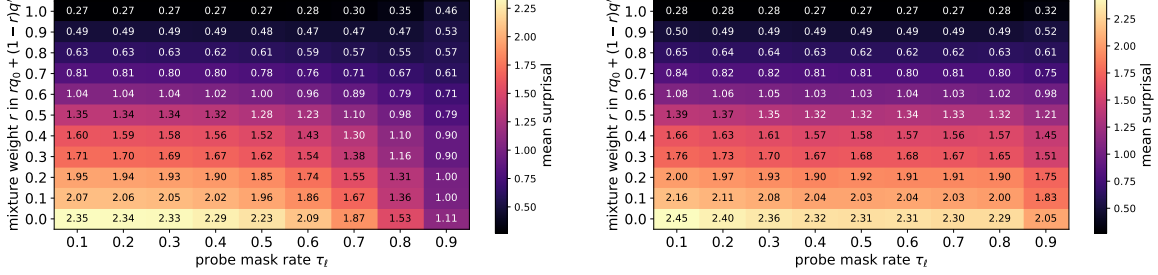
In this subsection, we discuss two practical variants of the proposed MaskDiff-AD framework. First, for small-scale categorical datasets, especially when many coordinates have binary or low-cardinality state spaces, we introduce a non-parametric version of the reconstruction score that estimates masked-coordinate conditional probabilities directly from normal training samples. This avoids the training of parametric MDMs. Second, when a pre-trained MDM is unavailable and one does not need to re-train a generic MDM, we provide a slightly different alternative loss to Eq. (2), for training the predictive models $p_{\hat{\theta}}^j(\cdot | \tilde{\mathbf{x}})$. This objective is more aligned with our anomaly score and can be useful especially for single-probe scoring.

Non-parametric reconstruction score. For a probe-masked view $\tilde{\mathbf{x}}$, instead of training a predictive parametric model $\{p_{\hat{\theta}}^j(\cdot | \mathbf{x}_t), j = 1, \dots, d\}$ to compute the anomaly score, we can also adopt the kernel-smoothed empirical conditional distribution as follows. Recall that $M(\tilde{\mathbf{x}})$ and $V(\tilde{\mathbf{x}})$ denote its masked and visible coordinate sets, respectively. Specifically, for each normal training sample $\mathbf{x}^{(n)} \in \mathcal{D}_{\text{tr}}$, define the visible-coordinate Hamming distance between $\mathbf{x}^{(n)}$ and $\tilde{\mathbf{x}}$ as

$$d_{\text{vis}}(\tilde{\mathbf{x}}, \mathbf{x}^{(n)}) := \sum_{r \in V(\tilde{\mathbf{x}})} \mathbf{1}\{\tilde{x}_r \neq x_r^{(n)}\}.$$

Then we estimate the reconstruction probability by

$$\hat{p}_{\text{NP}}^j(x_j = a | \tilde{\mathbf{x}}) := \frac{\sum_{n=1}^N \mathbf{1}\{x_j^{(n)} = a\} K_{\lambda}(\tilde{\mathbf{x}}, \mathbf{x}^{(n)})}{\sum_{n=1}^N K_{\lambda}(\tilde{\mathbf{x}}, \mathbf{x}^{(n)})}, \quad \forall j \in M(\tilde{\mathbf{x}}), a \in \mathcal{X}_j. \quad (7)$$



(a) Non-parametric score $\mathbb{E}[-\log \hat{p}_{\text{NP}}^j(x_j | \tilde{\mathbf{x}})]$ (b) Parametric score $\mathbb{E}[-\log p_{\hat{\theta}}^j(x_j | \tilde{\mathbf{x}})]$

Figure 2: Synthetic heatmaps of the expectation of non-parametric and parametric reconstruction anomaly score under the mixture $\mu_r = rq_0 + (1-r)q'$. Here, q_0 denotes the normal distribution over length-40 binary vectors, generated by drawing $S \sim \text{Bernoulli}(0.5)$ and making each coordinate a noisy copy of S with an 8% bit-flip probability. The anomaly distribution q' follows the same construction except that the target coordinate j is flipped relative to S , preserving its marginal while changing its conditional relationship with the visible context. For each $\mathbf{x} \sim \mu_r$, we mask coordinates at rate $1 - \alpha_{\tau_\ell}$ and then force the target coordinate j to be masked.

Here $K_\lambda(\tilde{\mathbf{x}}, \mathbf{x}^{(n)}) = \exp(-\lambda d_{\text{vis}}(\tilde{\mathbf{x}}, \mathbf{x}^{(n)}))$ is the kernel weight and $\lambda > 0$ is a pre-specified bandwidth parameter. The non-parametric anomaly score can be computed similarly as in Algorithm 1 by replacing the parametric predictive model $p_{\hat{\theta}}^j(\cdot | \mathbf{x}_t)$ with the non-parametric model in Eq. (7). The algorithm is given in Algorithm 2 in the Appendix for completeness.

To illustrate the non-parametric MaskDiff-AD score and compare it with the parametric score in Eq. (6), we evaluate both on a synthetic setting with varying anomaly levels in Figure 2, where $r = 0$ (bottom rows in each heatmap) corresponds to fully anomalous samples and $r = 1$ (top rows in each heatmap) to fully nominal samples. As samples move away from the normal distribution, the reconstruction posterior assigned to the true masked value decreases and the corresponding surprisal increases. This implies that both parametric and non-parametric scores can identify anomalous samples; the non-parametric score is comparable at smaller mask rates, while the parametric score becomes more effective at larger mask rates. For small datasets with simple discrete structure, however, the non-parametric version may be preferable because it requires no model training.

An alternative training objective. When a pre-trained MDM is available, MaskDiff-AD can be applied directly using the trained model without additional training. When such a model is unavailable and the goal is anomaly detection, it is not always necessary to train a generic MDM over all diffusion times. Instead, it suffices to learn the conditional distributions needed for the reconstruction score at the probe levels used at test time. To this end, we may also choose to train a time-conditioned predictive model $p_{\theta_{\text{rec}}}^j(\cdot | \tilde{\mathbf{x}}, \ell)$, which estimates the distribution of the clean coordinate x_j given a masked view $\tilde{\mathbf{x}}$ and the probe-level index ℓ . Specifically, for each normal training sample $\mathbf{x}^{(n)} \in \mathcal{D}_{\text{tr}}$ and each probe level τ_ℓ , we draw a masked view $\tilde{\mathbf{x}}^{(\ell, n)} \sim q_{\tau_\ell}(\cdot | \mathbf{x}^{(n)})$. We then fit the predictive model by minimizing the average masked reconstruction loss

$$\mathcal{L}_{\text{rec}}(\theta_{\text{rec}}) = -\frac{1}{NL} \sum_{n=1}^N \sum_{\ell=1}^L \frac{1}{|M(\tilde{\mathbf{x}}^{(\ell, n)})| \vee 1} \sum_{j \in M(\tilde{\mathbf{x}}^{(\ell, n)})} \log p_{\theta_{\text{rec}}}^j(x_j^{(n)} | \tilde{\mathbf{x}}^{(\ell, n)}, \ell). \quad (8)$$

This objective directly matches the test-time reconstruction score: the model is trained to predict only the coordinates that are masked in the probe views, and the loss is normalized per view to make different masking levels comparable. Averaging over $\ell = 1, \dots, L$ trains the model for the full multi-probe score used in Eq. (6); for single-probe scoring, one can set $L = 1$ and train only at

the chosen probe level. In this sense, the objective is tailored to anomaly scoring rather than to general-purpose masked diffusion generation.

The training loss in Eq. (8) closely resembles that of MDM in Eq. (2), with two key distinctions. First, our \mathcal{L}_{rec} is normalized by the number of masked coordinates, whereas this normalization is replaced with a time-dependent weight $w(t) = \alpha'_t/(1 - \alpha_t)$ in the standard MDM loss. Second, the loss in Eq. (8) is only computed with the fixed L mask levels that will be used in detection. This seemingly minor difference reflects the distinct objectives of the two settings. For sampling, [15, 42] showed that the MDM loss admits a clear interpretation as the KL divergence between probability paths, and minimizing it ensures effective generation along the diffusion trajectory. In contrast, for anomaly detection, our normalized \mathcal{L}_{rec} is directly aligned with the test-time scoring used in MaskDiff-AD. Furthermore, the loss \mathcal{L}_{rec} is expected to be trained exclusively on nominal data, while a pre-trained MDM might be trained on a more diverse dataset as in general-purpose language modeling.

3.3 Performance Guarantees

In this subsection, we provide some theoretical insights for the Type-I and Type-II errors of the proposed algorithm under a well-specified reconstruction model. Let $q^j(\cdot | \tilde{\mathbf{x}}, \tau_\ell)$ denote the oracle conditional distribution at probe level τ_ℓ , and let the corresponding oracle reconstruction score be

$$S^*(\mathbf{x}) := \frac{1}{L} \sum_{\ell=1}^L \mathbb{E}_{\tilde{\mathbf{x}} \sim q_{\tau_\ell}(\cdot | \mathbf{x})} \left[-\frac{1}{|M(\tilde{\mathbf{x}})| \vee 1} \sum_{j \in M(\tilde{\mathbf{x}})} \log q^j(x_j | \tilde{\mathbf{x}}, \tau_\ell) \right]. \quad (9)$$

We also define

$$S_{\text{rec}}^*(\mathbf{x}) := \frac{1}{L} \sum_{\ell=1}^L \mathbb{E}_{\tilde{\mathbf{x}} \sim q_{\tau_\ell}(\cdot | \mathbf{x})} \left[-\frac{1}{|M(\tilde{\mathbf{x}})| \vee 1} \sum_{j \in M(\tilde{\mathbf{x}})} \log p_{\hat{\theta}}^j(x_j | \tilde{\mathbf{x}}, \tau_\ell) \right], \quad (10)$$

which is the same quantity as $S^*(\mathbf{x})$ except when the reconstruction model is imperfect. If we define $\Delta_{\text{KL}}(\mathbf{x}) := S_{\text{rec}}^*(\mathbf{x}) - S^*(\mathbf{x})$, note that

$$\mathbb{E}_{\mathbf{x} \sim q_0}[\Delta_{\text{KL}}(\mathbf{x})] = \frac{1}{L} \sum_{\ell=1}^L \mathbb{E}_{\tilde{\mathbf{x}} \sim q_{\tau_\ell}} \left[\frac{1}{|M(\tilde{\mathbf{x}})| \vee 1} \sum_{j \in M(\tilde{\mathbf{x}})} KL(q^j(\cdot | \tilde{\mathbf{x}}, \tau_\ell) || p_{\hat{\theta}}^j(\cdot | \tilde{\mathbf{x}}, \tau_\ell)) \right] > 0.$$

Further, when $p_{\hat{\theta}}^j$ is well-trained with the loss in Eq. (8), we have $\mathbb{E}_{\mathbf{x} \sim q_0}[\Delta_{\text{KL}}(\mathbf{x})] \leq \epsilon$ for some small ϵ . Finally, we let $S_{\text{rec}}(\mathbf{x})$ be the anomaly score in Eq. (6), which is a sampled version (or realization) of $S_{\text{rec}}^*(\mathbf{x})$. The following theorem summarizes the guarantee on Type-I/Type-II errors of the anomaly detector. The proof can be found in Appendix C.

Theorem 1 (Detection performance). *We assume there exists constant $C > 0$ such that for all j , all probe levels τ_ℓ , and all masked views $\tilde{\mathbf{x}}$, the trained and true models satisfy $-\log p_{\hat{\theta}_{\text{rec}}}^j(x_j | \tilde{\mathbf{x}}, \tau_\ell) \in [0, C]$, and $-\log q^j(x_j | \tilde{\mathbf{x}}, \tau_\ell) \in [0, C]$. We also assume that the training loss is small such that $\mathbb{E}_{\mathbf{x} \sim q_0}[\Delta_{\text{KL}}(\mathbf{x})] \leq \epsilon$. Then, for a fixed threshold γ , we have*

- *Type-I error: for normal data $\mathbf{x} \sim q_0$, let $\mu_0^* := \mathbb{E}_{\mathbf{x} \sim q_0}[S^*(\mathbf{x})]$ be the oracle normal mean. Then,*

$$\mathbb{P}_{\mathbf{x} \sim q_0}(S_{\text{rec}}(\mathbf{x}) > \gamma) \leq 3 \exp \left(-\frac{\min\{L, K\}(\gamma - \mu_0^* - \epsilon)^2}{18C^2} \right).$$

- *Type-II error: for anomalous data $\mathbf{x} \sim q'$, let $\mu_1^* := \mathbb{E}_{q'}[S^*(\mathbf{x})]$. Assume that $\mu_1^* - \mu_0^* > 0$ and no estimation error, i.e., $\varepsilon = 0$. Then,*

$$\mathbb{P}_{\mathbf{x} \sim q'}(S_{\text{rec}}(\mathbf{x}) \leq \gamma) \leq 2 \exp\left(-\frac{\min\{L, K\}(\mu_1^* - \gamma)^2}{2C^2}\right).$$

Remark 2. *The gap between μ_0^* and μ_1^* increases as q' deviates further from q_0 . To build some intuition, fix a large τ_ℓ and consider the regime where $|M(\tilde{\mathbf{x}})|$ is also large and fixed. Then,*

$$\begin{aligned} \mu_0^* &\approx \mathbb{E}_j \mathbb{E}_{\mathbf{x} \sim q_0, \tilde{\mathbf{x}} \sim q_{\tau_\ell} | 0(\cdot | \mathbf{x})} [-\log q^j(x_j | \tilde{\mathbf{x}}, \tau_\ell)] = \mathbb{E}_j \mathbb{E}_{\tilde{\mathbf{x}} \sim q_{\tau_\ell}} H(q^j(\cdot | \tilde{\mathbf{x}}, \tau_\ell)), \\ \mu_1^* &\approx \mathbb{E}_j \mathbb{E}_{\mathbf{x} \sim q', \tilde{\mathbf{x}} \sim q_{\tau_\ell} | 0(\cdot | \mathbf{x})} [-\log q^j(x_j | \tilde{\mathbf{x}}, \tau_\ell)] = \mathbb{E}_j \mathbb{E}_{\tilde{\mathbf{x}} \sim q'_{\tau_\ell}} H(q'^j(\cdot | \tilde{\mathbf{x}}, \tau_\ell), q^j(\cdot | \tilde{\mathbf{x}}, \tau_\ell)), \end{aligned}$$

where $H(\cdot)$ denotes entropy, q'_{τ_ℓ} is the forward masking distribution initialized from q' , and $H(q', q)$ denotes cross-entropy, defined as $H(q', q) = H(q') + KL(q' || q)$. Since the diffusion process implies $q'_{\tau_\ell} \approx q_{\tau_\ell}$ for large τ_ℓ , the two terms become comparable. For such a case, the dominant contribution to $\mu_1^* - \mu_0^*$ arises from the KL divergence between the corresponding reconstruction distributions. This separation ensures reliable detection when γ is chosen appropriately.

4 Numerical Experiments

Numerical setup. We evaluate MaskDiff-AD on *eighteen* real-world datasets, including *thirteen* fully discrete tabular data, *one* mixed-type tabular data (with both categorical variables and continuous variables), and *four* discrete text sequences. The summary of datasets is shown in Table 3 in Appendix B.1. All experiments follow the normal-only training of the anomaly detection protocol: during training, each method has access only to samples from the normal class; anomalous samples are used only for test-time evaluation. On tabular data, features are represented as discrete symbols, with continuous features discretized when necessary. On text data, each document is converted into a fixed-length token sequence and masked reconstruction is performed at the token level. This allows the same forward-only scoring principle to be applied across different discrete data modalities.

For MaskDiff-AD, we use fixed hyperparameters across datasets rather than validation-based or per-dataset tuning. We use the standard linear absorbing schedule $\alpha_t = 1 - t$, so the probe level τ_ℓ has mask probability $1 - \alpha_{\tau_\ell} = \tau_\ell$. The parametric tabular and text models use the uniform probe grid $\tau_\ell \in \{0.1, 0.2, \dots, 0.9\}$, while the non-parametric tabular model uses $\tau_\ell \in \{0.15, 0.30, 0.45, 0.60\}$. For tabular data, the parametric reconstruction score averages over $K = 16$ masked probe views at each probe level. The non-parametric model uses the visible-coordinate Hamming kernel with bandwidth $\lambda = 1$, takes all normal training samples as the reference set, and averages over 8 masked probe views at each probe level. For text data, we use the GPT-2 [43] tokenizer only, without using pretrained GPT-2 weights, and we average the reconstruction score over 24 independently generated masked probe views at each probe level. Model architectures, optimization details, and additional implementation hyperparameters are provided in Appendix B.3.

Baselines and metrics. We compare against classical anomaly detection baselines, DTE-based variants, and recent tabular or text anomaly detection methods when applicable. Specifically, for tabular data, we compare against 12 baseline methods, including COPOD [25], DeepSVDD [44], DTE-Categorical [21], DTE-InvGamma [21], DTE-Gaussian [21], DRL [31], ECOD [24], GOAD [45], Hamming k -nearest neighbors (Hamming- k NN) [22], ICL [29], IForest [23], and MCM [27]. For text data, we compare with DATE [46], FATE [47], and several embedding-based baselines. Specifically, we use BERT embeddings [48] and OpenAI text embeddings [49] as fixed document

Table 1: Average ranks on tabular datasets over five random seeds. Ranks are computed separately for ROC-AUC and PR-AUC across datasets, and the overall rank is the average of the two metric-specific ranks.

Method	Overall Rank	ROC-AUC Rank	PR-AUC Rank
Parametric MaskDiff-AD	3.929	3.714	4.143
Non-parametric MaskDiff-AD	4.929	4.857	5.000
DTE-Gaussian	5.286	4.929	5.643
Hamming-kNN	6.250	6.000	6.500
DTE-Categorical	6.357	5.214	7.500
DRL	7.429	7.857	7.000
ECOD	7.857	7.429	8.286
COPOD	7.929	7.857	8.000
GOAD	8.464	8.500	8.429
DTE-InvGamma	8.571	9.429	7.714
ICL	8.786	9.286	8.286
MCM	8.821	9.214	8.429
DeepSVDD	9.679	10.786	8.571
IForest	10.714	9.929	11.500

representations, followed by LOF [50], DeepSVDD [44], ECOD [24], Isolation Forest [23], SO-GAAL [51], AE [52], VAE [53], and LUNAR [54]. We report ROC-AUC and PR-AUC: ROC-AUC measures global ranking quality, and PR-AUC summarizes the precision–recall trade-off and is especially informative under class imbalance. Detailed definitions are provided in Appendix B.2.

Results. Table 1, summarized from the results in Tables 6 and 7 in the Appendix, shows that our reconstruction-based variants are overall the strongest on tabular data. In particular, the parametric reconstruction anomaly score achieves the best average overall rank (3.93), and the non-parametric variant also ranks among the top methods. Among the baselines, **Hamming-kNN** is the strongest competitor, whereas **DTE-Gaussian** is the best-performing DTE variant. It is worthwhile mentioning that the DTE variants method compared here is implemented by embedding the discrete features into a continuous space and applying Gaussian DTE there. This represents a natural application of the DTE method in discrete data; yet this no longer defines a diffusion process on the original categorical space. The resulting time posterior depends on the geometry induced by the chosen embedding and may not faithfully preserve the distributional structure and inter-feature dependencies of normal data. In contrast, our proposed method operates directly in the discrete state space and achieves stronger overall performance, as reflected by its best average rank. This indicates that reconstruction-based scores are more reliable than time-based scores in the tabular setting.

For text data, Table 2 shows that the proposed parametric reconstruction score is especially effective on short spam-detection datasets. It achieves the best performance on Email Spam and SMS Spam, outperforming both end-to-end text anomaly detectors such as DATE and embedding-based baselines. On AGNews and YelpReview, however, our method is less competitive than the strongest OpenAI-embedding baselines, suggesting that long or semantically richer text sequences may require more specialized sequence architectures or text-specific training. Overall, these results indicate that masked reconstruction serves as a promising signal for identifying anomalous discrete sequences, while also highlighting an important direction for improving MaskDiff-AD on longer text data.

Sensitivity analysis on probe level τ . We further study the effect of the probe level using the Vehicle Claims dataset. Figure 3 reports the ROC-AUC of the proposed parametric score when computed from a single probe mask rate τ . The ROC-AUC first increases at small τ and then decreases when too much context is removed. This suggests a trade-off: at small τ the

Table 2: Anomaly detection performance on NLP datasets.

Method	AGNews		Email Spam		SMS Spam		YelpReview	
	ROC-AUC	PR-AUC	ROC-AUC	PR-AUC	ROC-AUC	PR-AUC	ROC-AUC	PR-AUC
Parametric MaskDiff-AD	76.03	31.11	97.55	88.87	95.69	72.15	58.82	20.42
COPOD	50.91	11.46	53.46	18.31	86.77	31.76	54.54	18.98
ECOD	49.19	11.06	55.61	19.39	86.07	31.31	54.65	19.02
Hamming-kNN	50.64	11.80	56.68	27.11	87.26	32.70	58.55	21.76
Isolation Forest	52.30	11.90	57.65	16.61	88.47	34.75	52.33	11.92
CVDD	60.46	12.96	93.40	53.53	47.82	7.12	53.45	17.11
DATE	81.20	39.96	96.97	88.85	93.98	61.12	60.92	21.49
FATE	77.56	27.87	90.61	55.29	62.62	12.57	59.45	21.12
BERT + AE	72.00	22.32	47.39	29.37	69.18	19.14	64.41	25.25
BERT + DeepSVDD	66.71	21.60	69.37	21.17	58.59	11.78	58.71	21.74
BERT + ECOD	63.18	16.16	70.52	20.77	56.06	11.56	63.26	21.97
BERT + iForest	61.24	15.59	67.79	18.94	50.53	9.94	59.71	22.03
BERT + LOF	74.32	25.49	74.82	23.70	71.90	18.37	65.73	26.29
BERT + LUNAR	76.94	27.17	84.17	35.71	69.53	18.17	65.22	26.09
BERT + SO-GAAL	44.89	10.33	44.40	11.30	33.28	7.14	47.12	24.40
BERT + VAE	67.73	18.78	47.37	22.47	60.82	13.60	64.41	23.31
OpenAI + AE	83.26	40.22	76.51	55.80	55.11	10.30	85.24	70.63
OpenAI + DeepSVDD	46.80	10.62	44.15	11.95	34.91	7.21	53.73	18.93
OpenAI + ECOD	76.38	32.94	92.63	55.97	43.17	8.21	59.84	86.39
OpenAI + iForest	52.13	12.78	69.37	32.83	37.51	7.72	58.71	25.27
OpenAI + LOF	89.05	54.43	92.63	59.67	78.62	24.50	87.33	57.10
OpenAI + LUNAR	92.26	69.18	93.43	58.10	71.89	16.40	94.52	45.24
OpenAI + SO-GAAL	59.45	15.38	44.40	10.96	56.71	12.13	50.82	27.35
OpenAI + VAE	81.44	36.59	52.73	56.04	42.59	8.12	61.63	84.67

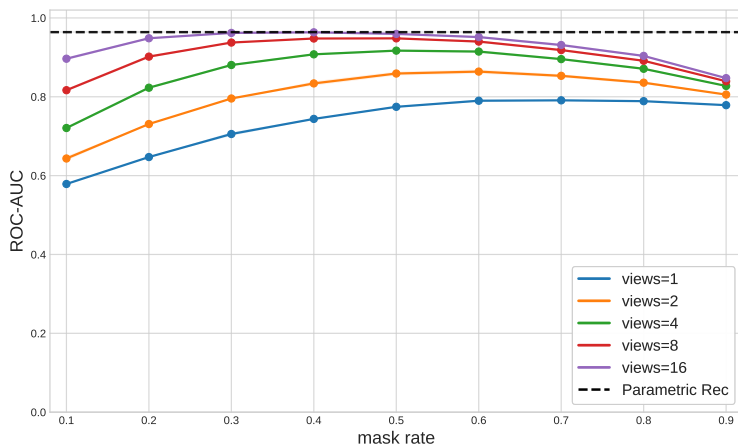


Figure 3: Sensitivity of the ROC-AUC to the probe rate mask rate on the Vehicle Claims dataset. Each solid curve uses a single probe mask rate τ and averages over $K \in \{1, 2, 4, 8, 16\}$ masked views. The dashed line denotes our default multi-probe parametric reconstruction score, which aggregates over the full uniform probe grid.

algorithm masks too few coordinates to expose anomalous dependencies, while at large τ the missing context makes reconstruction difficult for both normal and anomalous samples. Additional results in Appendix B.5 show that the best single probe level can differ across datasets. Therefore, we use a fixed multi-probe score in the main experiments, aggregating over a uniform grid of probe levels instead of tuning τ separately for each dataset.

5 Conclusion and Discussions

We proposed MaskDiff-AD, a masked diffusion-based anomaly detection framework for discrete data. The method uses a trained masked diffusion model for anomaly scoring: a test sample is randomly masked at multiple probe levels, and its anomaly score is the average reconstruction surprisal of the masked entries. This design directly leverages the discrete structure of the data and is computationally efficient to compute. Our theoretical analysis provided Type-I and Type-II error insights under well-specified reconstruction models, and our experiments showed competitive performance across eighteen tabular and text datasets. One limitation is that the method depends on the quality of the learned masked conditionals and on the choice of probe levels, although multi-probe averaging helps to reduce this sensitivity. In addition, its performance on long text sequences is currently less competitive, which may be partly due to the simple text modeling and token-level architecture used in our experiments. Future work includes adaptive selection of probe levels, text-specific architectures and training strategies for long sequences, extensions to structured discrete objects such as graphs and molecules, and tighter theory connecting masked reconstruction with distributional divergences between nominal and anomalous data.

References

- [1] Varun Chandola, Arindam Banerjee, and Vipin Kumar. Anomaly detection: A survey. *ACM computing surveys (CSUR)*, 41(3):1–58, 2009.
- [2] Lukas Ruff, Jacob R Kauffmann, Robert A Vandermeulen, Grégoire Montavon, Wojciech Samek, Marius Kloft, Thomas G Dietterich, and Klaus-Robert Müller. A unifying review of deep and shallow anomaly detection. *Proceedings of the IEEE*, 109(5):756–795, 2021.
- [3] Guansong Pang, Chunhua Shen, Longbing Cao, and Anton Van Den Hengel. Deep learning for anomaly detection: A review. *ACM Computing Surveys (CSUR)*, 54(2):1–38, 2021.
- [4] Osman Salem, Alexey Guerassimov, Ahmed Mehaoua, Anthony Marcus, and Borko Furht. Sensor fault and patient anomaly detection and classification in medical wireless sensor networks. In *2013 IEEE International Conference on Communications (ICC)*, pages 4373–4378. IEEE, 2013.
- [5] Girik Pachauri and Sandeep Sharma. Anomaly detection in medical wireless sensor networks using machine learning algorithms. *Procedia Computer Science*, 70:325–333, 2015.
- [6] Mohiuddin Ahmed, Abdun Naser Mahmood, and Md Rafiqul Islam. A survey of anomaly detection techniques in financial domain. *Future Generation Computer Systems*, 55:278–288, 2016.
- [7] Gian Antonio Susto, Matteo Terzi, and Alessandro Beghi. Anomaly detection approaches for semiconductor manufacturing. *Procedia Manufacturing*, 11:2018–2024, 2017.
- [8] Katherine Fraser, Samuel Homiller, Rashmish K Mishra, Bryan Ostdiek, and Matthew D Schwartz. Challenges for unsupervised anomaly detection in particle physics. *Journal of High Energy Physics*, 2022(3):66, 2022.
- [9] Takehisa Yairi, Yoshinobu Kawahara, Ryohei Fujimaki, Yuichi Sato, and Kazuo Machida. Telemetry-mining: a machine learning approach to anomaly detection and fault diagnosis

- for space systems. In *2nd IEEE International Conference on Space Mission Challenges for Information Technology (SMC-IT'06)*, pages 8–pp. IEEE, 2006.
- [10] Ayman Taha and Ali S Hadi. Anomaly detection methods for categorical data: A review. *ACM Computing Surveys (CSUR)*, 52(2):1–35, 2019.
- [11] Songqiao Han, Xiyang Hu, Hailiang Huang, Minqi Jiang, and Yue Zhao. Adbench: Anomaly detection benchmark. *Advances in Neural Information Processing Systems*, 35:32142–32159, 2022.
- [12] Yuangang Li, Jiaqi Li, Zhuo Xiao, Tiankai Yang, Yi Nian, Xiyang Hu, and Yue Zhao. Nlp-adbench: Nlp anomaly detection benchmark. *Findings of the Association for Computational Linguistics: EMNLP 2025*, 2025.
- [13] Jascha Sohl-Dickstein, Eric Weiss, Niru Maheswaranathan, and Surya Ganguli. Deep unsupervised learning using nonequilibrium thermodynamics. In *International conference on machine learning*, pages 2256–2265. pmlr, 2015.
- [14] Jonathan Ho, Ajay Jain, and Pieter Abbeel. Denoising diffusion probabilistic models. *Advances in Neural Information Processing Systems*, 33:6840–6851, 2020.
- [15] Subham S Sahoo, Marianne Arriola, Yair Schiff, Aaron Gokaslan, Edgar Marroquin, Justin T Chiu, Alexander Rush, and Volodymyr Kuleshov. Simple and effective masked diffusion language models. *Advances in Neural Information Processing Systems*, 37:130136–130184, 2024.
- [16] Jacob Austin, Daniel D Johnson, Jonathan Ho, Daniel Tarlow, and Rianne Van Den Berg. Structured denoising diffusion models in discrete state-spaces. *Advances in Neural Information Processing Systems*, 34:17981–17993, 2021.
- [17] Kaiwen Zheng, Yongxin Chen, Hanzi Mao, Ming-Yu Liu, Jun Zhu, and Qinsheng Zhang. Masked diffusion models are secretly time-agnostic masked models and exploit inaccurate categorical sampling. In *International Conference on Learning Representations (ICLR)*, 2025.
- [18] Mihir Prabhudesai, Mengning Wu, Amir Zadeh, Katerina Fragkiadaki, and Deepak Pathak. Diffusion beats autoregressive in data-constrained settings. In *The Thirty-ninth Annual Conference on Neural Information Processing Systems*, 2025.
- [19] Michael Cardei, Jacob K Christopher, Thomas Hartvigsen, Bhavya Kailkhura, and Ferdinando Fioretto. Constrained discrete diffusion. *arXiv preprint arXiv:2503.09790*, 2025.
- [20] Masatoshi Uehara, Yulai Zhao, Tommaso Biancalani, and Sergey Levine. Understanding reinforcement learning-based fine-tuning of diffusion models: A tutorial and review. *arXiv preprint arXiv:2407.13734*, 2024.
- [21] Victor Liversoche, Vineet Jain, Yashar Hezaveh, and Siamak Ravanbakhsh. On diffusion modeling for anomaly detection. In *The Twelfth International Conference on Learning Representations*, 2024.
- [22] Sridhar Ramaswamy, Rajeev Rastogi, and Kyuseok Shim. Efficient algorithms for mining outliers from large data sets. *SIGMOD Record*, 29(2):427–438, June 2000.
- [23] Fei Tony Liu, Kai Ming Ting, and Zhi-Hua Zhou. Isolation forest. In *Proceedings of the 2008 Eighth IEEE International Conference on Data Mining, ICDM '08*, page 413–422, USA, 2008. IEEE Computer Society.

- [24] Zheng Li, Yue Zhao, Xiyang Hu, Nicola Botta, Cezar Ionescu, and George H. Chen. ECOD: Unsupervised outlier detection using empirical cumulative distribution functions. *IEEE Transactions on Knowledge and Data Engineering*, 35(12):12181–12193, 2023.
- [25] Zheng Li, Yue Zhao, Nicola Botta, Cezar Ionescu, and Xiyang Hu. Copod: Copula-based outlier detection. In *2020 IEEE International Conference on Data Mining (ICDM)*, page 1118–1123. IEEE, November 2020.
- [26] Ajay Chawda, Stefanie Grimm, and Marius Kloft. Unsupervised anomaly detection for auditing data and impact of categorical encodings. *arXiv preprint arXiv:2210.14056*, 2022.
- [27] Jiaxin Yin, Yuanyuan Qiao, Zitang Zhou, Xiangchao Wang, and Jie Yang. MCM: Masked cell modeling for anomaly detection in tabular data. In *The Twelfth International Conference on Learning Representations*, 2024.
- [28] Hugo Thimonier, Fabrice Popineau, Arpad Rimmel, and Bich-Liên Doan. Beyond individual input for deep anomaly detection on tabular data. In *Proceedings of the 41st International Conference on Machine Learning*, volume 235 of *Proceedings of Machine Learning Research*, pages 48097–48123. PMLR, 21–27 Jul 2024.
- [29] Tom Shenkar and Lior Wolf. Anomaly detection for tabular data with internal contrastive learning. In *International Conference on Learning Representations*, 2022.
- [30] Leman Akoglu, Hanghang Tong, Jilles Vreeken, and Christos Faloutsos. Fast and reliable anomaly detection in categorical data. In *Proceedings of the 21st ACM International Conference on Information and Knowledge Management, CIKM '12*, page 415–424, New York, NY, USA, 2012. Association for Computing Machinery.
- [31] Hangting Ye, He Zhao, Wei Fan, Mingyuan Zhou, Dan dan Guo, and Yi Chang. DRL: Decomposed representation learning for tabular anomaly detection. In *The Thirteenth International Conference on Learning Representations*, 2025.
- [32] Mayu Sakurada and Takehisa Yairi. Anomaly detection using autoencoders with nonlinear dimensionality reduction. In *Proceedings of the MLSDA 2014 2nd workshop on machine learning for sensory data analysis*, pages 4–11, 2014.
- [33] Jinwon An and Sungzoon Cho. Variational autoencoder based anomaly detection using reconstruction probability. *Special lecture on IE*, 2(1):1–18, 2015.
- [34] Bo Zong, Qi Song, Martin Renqiang Min, Wei Cheng, Cristian Lumezanu, Daeki Cho, and Haifeng Chen. Deep autoencoding gaussian mixture model for unsupervised anomaly detection. In *International Conference on Learning Representations*, 2018.
- [35] Thomas Schlegl, Philipp Seeböck, Sebastian M. Waldstein, Ursula Schmidt-Erfurth, and Georg Langs. Unsupervised anomaly detection with generative adversarial networks to guide marker discovery. In *Information Processing in Medical Imaging*, pages 146–157. Springer, 2017.
- [36] Samet Akcay, Amir Atapour-Abarghouei, and Toby P Breckon. Ganomaly: Semi-supervised anomaly detection via adversarial training. In *Asian conference on computer vision*, pages 622–637. Springer, 2018.

- [37] Marco Rudolph, Bastian Wandt, and Bodo Rosenhahn. Same same but different: Semi-supervised defect detection with normalizing flows. In *Proceedings of the IEEE/CVF winter conference on applications of computer vision*, pages 1907–1916, 2021.
- [38] Jing Liu, Zhenchao Ma, Zepu Wang, Chenxuanyin Zou, Jiayang Ren, Zehua Wang, Liang Song, Bo Hu, Yang Liu, and Victor Leung. A survey on diffusion models for anomaly detection. *arXiv preprint arXiv:2501.11430*, 2025.
- [39] Julian Wyatt, Adam Leach, Sebastian M Schmon, and Chris G Willcocks. Anoddpm: Anomaly detection with denoising diffusion probabilistic models using simplex noise. In *Proceedings of the IEEE/CVF conference on computer vision and pattern recognition*, pages 650–656, 2022.
- [40] Arian Mousakhan, Thomas Brox, and Jawad Tayyub. Anomaly detection with conditioned denoising diffusion models. In *DAGM German Conference on Pattern Recognition*, pages 181–195. Springer, 2024.
- [41] Hui Zhang, Zheng Wang, Dan Zeng, Zuxuan Wu, and Yu-Gang Jiang. Diffusionad: Norm-guided one-step denoising diffusion for anomaly detection. *IEEE transactions on pattern analysis and machine intelligence*, 2025.
- [42] Jiaxin Shi, Kehang Han, Zhe Wang, Arnaud Doucet, and Michalis Titsias. Simplified and generalized masked diffusion for discrete data. In *The Thirty-eighth Annual Conference on Neural Information Processing Systems*, 2024.
- [43] Alec Radford, Jeffrey Wu, Rewon Child, David Luan, Dario Amodei, Ilya Sutskever, et al. Language models are unsupervised multitask learners. *OpenAI blog*, 1(8):9, 2019.
- [44] Lukas Ruff, Robert Vandermeulen, Nico Goernitz, Lucas Deecke, Shoaib Ahmed Siddiqui, Alexander Binder, Emmanuel Müller, and Marius Kloft. Deep one-class classification. In Jennifer Dy and Andreas Krause, editors, *Proceedings of the 35th International Conference on Machine Learning*, volume 80 of *Proceedings of Machine Learning Research*, pages 4393–4402. PMLR, 10–15 Jul 2018.
- [45] Liron Bergman and Yedid Hoshen. Classification-based anomaly detection for general data. In *International Conference on Learning Representations (ICLR)*, 2020.
- [46] Andrei Manolache, Florin Brad, and Elena Burceanu. DATE: Detecting anomalies in text via self-supervision of transformers. In Kristina Toutanova, Anna Rumshisky, Luke Zettlemoyer, Dilek Hakkani-Tur, Iz Beltagy, Steven Bethard, Ryan Cotterell, Tanmoy Chakraborty, and Yichao Zhou, editors, *Proceedings of the 2021 Conference of the North American Chapter of the Association for Computational Linguistics: Human Language Technologies*, pages 267–277, Online, June 2021. Association for Computational Linguistics.
- [47] Anindya Sundar Das, Aravind Ajay, Sriparna Saha, and Monowar Bhuyan. Few-shot anomaly detection in text with deviation learning. In *International Conference on Neural Information Processing*, pages 425–438. Springer, 2023.
- [48] Jacob Devlin, Ming-Wei Chang, Kenton Lee, and Kristina Toutanova. BERT: Pre-training of deep bidirectional transformers for language understanding. In Jill Burstein, Christy Doran, and Tamar Solorio, editors, *Proceedings of the 2019 Conference of the North American Chapter of the Association for Computational Linguistics: Human Language Technologies, Volume 1 (Long and Short Papers)*, pages 4171–4186, Minneapolis, Minnesota, June 2019. Association for Computational Linguistics.

- [49] OpenAI. New embedding models and api updates. <https://openai.com/index/new-embedding-models-and-api-updates/>.
- [50] Markus M Breunig, Hans-Peter Kriegel, Raymond T Ng, and Jörg Sander. Lof: identifying density-based local outliers. In *Proceedings of the 2000 ACM SIGMOD international conference on Management of data*, pages 93–104, 2000.
- [51] Yezheng Liu, Zhe Li, Chong Zhou, Yuanchun Jiang, Jianshan Sun, Meng Wang, and Xiangnan He. Generative adversarial active learning for unsupervised outlier detection. *IEEE Transactions on Knowledge and Data Engineering*, 32(8):1517–1528, 2019.
- [52] Charu C. Aggarwal. *Outlier Analysis*. Springer, 2 edition, 2017.
- [53] Diederik P. Kingma and Max Welling. Auto-encoding variational bayes. *arXiv preprint arXiv:1312.6114*, 2013.
- [54] Adam Goodge, Bryan Hooi, See-Kiong Ng, and Wee Siong Ng. Lunar: Unifying local outlier detection methods via graph neural networks. *Proceedings of the AAAI Conference on Artificial Intelligence*, 36(6):6737–6745, Jun. 2022.

A Algorithmic Details

In this section, we provide the detailed algorithms for the two variants mentioned in Section 3.2. Algorithm 2 summarizes the non-parametric version of the MaskDiff-AD using the non-parametric score computed from Eq. (7). Algorithm 3 summarizes the training procedure when using the alternative training objective in Eq. (8).

Algorithm 2 Non-Parametric MaskDiff-AD

Input: Test sample \mathbf{x} ; normal-only training data \mathcal{D}_{tr} ; probe grids $\{\tau_\ell\}_{\ell=1}^L$; number of views per mask level K ; detection threshold γ .

Output: Anomaly label $\hat{y}(\mathbf{x}) \in \{0, 1\}$, where 1 indicates anomalous and 0 indicates normal.

- 1: **for** each $\ell = 1, \dots, L$ and $k = 1, \dots, K$ **do**
- 2: Sample the corresponding probe-masked view $\tilde{\mathbf{x}}^{(k,\ell)} \sim q_{\tau_\ell|0}(\cdot | \mathbf{x})$ according to Eq. (3).
- 3: Compute per-view reconstruction difficulty

$$s_{\text{rec}}^{\text{NP}}(\mathbf{x}; \tilde{\mathbf{x}}^{(\ell,k)}) = -\frac{1}{|M(\tilde{\mathbf{x}}^{(\ell,k)})| \vee 1} \sum_{j \in M(\tilde{\mathbf{x}}^{(\ell,k)})} \log \hat{p}_{\text{NP}}^j(x_j | \tilde{\mathbf{x}}^{(\ell,k)})$$

where $\hat{p}_{\text{NP}}^j(\cdot | \tilde{\mathbf{x}})$ is as in Eq. (7).

- 4: **end for**
- 5: Compute the aggregated anomaly score

$$S_{\text{rec}}^{\text{NP}}(\mathbf{x}) := \frac{1}{LK} \sum_{\ell=1}^L \sum_{k=1}^K s_{\text{rec}}^{\text{NP}}(\mathbf{x}; \tilde{\mathbf{x}}^{(\ell,k)}).$$

- 6: **return** Anomaly label $\hat{y}(\mathbf{x}) = \mathbf{1}\{S_{\text{rec}}^{\text{NP}}(\mathbf{x}) > \gamma\}$.
-

Algorithm 3 Training of Alternative Parametric Reconstruction Model

Input: Normal training set $D_{\text{tr}} = \{\mathbf{x}^{(n)}\}_{n=1}^N$, probe grids rates $\{\tau_\ell\}_{\ell=1}^L$, total epochs E , learning rate η .

Output: Trained reconstruction model $p_{\hat{\theta}_{\text{rec}}}^j(\cdot | \tilde{\mathbf{x}})$, $j = 1, \dots, d$.

- 1: Initialize reconstruction model $p_{\hat{\theta}_{\text{rec}}}^j$
 - 2: **for** epoch = 1, \dots , E **do**
 - 3: **for** each mask level $\ell = 1, \dots, L$ **do**
 - 4: Sample masked views $\tilde{\mathbf{x}}^{(\ell, n)} \sim q_{\tau_\ell|0}(\cdot | \mathbf{x}^{(n)})$, $n = 1, \dots, N$
 - 5: **end for**
 - 6: Compute the reconstruction loss $\mathcal{L}_{\text{rec}}(\theta_{\text{rec}})$ according to (8)
 - 7: Update parameters $\theta_{\text{rec}} \leftarrow \theta_{\text{rec}} - \eta \nabla_{\theta_{\text{rec}}} \mathcal{L}_{\text{rec}}(\theta_{\text{rec}})$
 - 8: **end for**
-

B Experiment Details

B.1 Datasets and Pre-processing

Table 3 summarizes the eighteen datasets we used for evaluating the proposed method. The datasets include thirteen categorical tabular datasets from ADBench [3], one mixed-type vehicle claims dataset from UADAD [26], and four text anomaly detection datasets from NLP-ADBench [12]. All experiments follow the normal-only anomaly detection protocol: anomaly labels are used only for constructing stratified splits and for test-time evaluation, but are never used for training the proposed method.

Table 3: Datasets overview.

Dataset Name	# Samples	# Features	% Anomaly	Data Type
AD [3]	3,279	1,555	14.00%	Categorical
AID362 [3]	4,279	114	1.40%	Categorical
APAS [3]	12,695	64	1.39%	Categorical
bank [3]	41,188	10	11.27%	Categorical
census [3]	299,285	33	6.20%	Categorical
Chess [3]	28,056	6	0.10%	Categorical
CMC [3]	1,473	8	1.97%	Categorical
CoverType [3]	581,012	44	0.47%	Categorical
probe [3]	64,759	6	6.43%	Categorical
R10 [3]	12,897	100	1.84%	Categorical
Solar [3]	1,066	11	4.03%	Categorical
U2R [3]	60,821	6	0.38%	Categorical
Vehicle claims [26]	268,255	18	21.15%	Mixed-type
w7a [3]	49,749	300	2.97%	Categorical
AGNews [12]	98,207	128	3.85%	NLP
Email spam [12]	3,578	256	4.08%	NLP
SMS spam [12]	4,672	128	3.30%	NLP
YelpReview [12]	316,924	256	5.66%	NLP

UADAD. We use the labeled vehicle claims dataset from the UADAD benchmark [26]. Following the main feature setting of that benchmark, we retain the following attributes:

Maker, Genmodel, Color, Reg_year, Bodytype, Runned_Miles,
 Engin_size, Gearbox, Fuel_type, Price, Seat_num, Door_num,
 issue, issue_id, repair_complexity, repair_hours, repair_cost.

The column `Label` is used only for splitting and evaluation, where `Label = 0` denotes a normal sample and `Label = 1` denotes an anomalous sample. We randomly split the full labeled dataset into 70% training and 30% testing using a stratified split with respect to `Label`. To match the unsupervised anomaly detection setting, only normal samples with `Label = 0` in the training split are used to train the model or build the reference set. The full test split, containing both normal and anomalous samples, is used for evaluation.

We treat the vehicle claims dataset as a mixed-type tabular dataset. Categorical attributes are kept as discrete symbols and encoded into integer IDs. Numerical attributes are discretized by quantile binning, where the bin boundaries are fitted using only the normal training samples and then applied to the test set. This yields a fully discrete representation for MaskDiff-AD and the corresponding discrete baselines.

ADBench. For the ADBench datasets [3], we also randomly split each full labeled dataset into 70% training and 30% testing using a stratified split with respect to the anomaly label. After the split, all anomalous samples in the training portion are removed, and only nominal training samples are used for model training or for constructing the non-parametric reference set. The test set is kept unchanged and contains both normal and anomalous samples. Thus, anomalous samples are never observed during training, and labels are used only for evaluation.

All ADBench datasets used in our experiments are treated as categorical tabular datasets. Each feature is represented as a discrete symbol and encoded into an integer ID. The same discrete representation is used for MaskDiff-AD and for tabular baselines whenever applicable.

NLP-ADBench. For the NLP anomaly detection datasets, we follow the official train/test split provided by NLP-ADBench [12], which uses 90% of the data for training and 10% for testing. As in the tabular experiments, only normal samples in the training split are used for training. The full test split, containing both normal and anomalous text samples, is used for computing anomaly scores and evaluation metrics.

For text preprocessing, we convert each raw text sample into a fixed-length discrete sequence using the GPT-2 tokenizer [43]. Our model does not use the pretrained GPT-2 language model or its pretrained token embeddings; the tokenizer is used only to map raw text into discrete token IDs.

Specifically, we use the GPT-2 tokenizer and apply right padding to obtain fixed-length token sequences. Since the original GPT-2 tokenizer does not provide dedicated padding or mask tokens, we add them when they are absent:

$$\langle \text{pad} \rangle, \quad \langle \text{m} \rangle.$$

Let \mathcal{V} denote the resulting tokenizer vocabulary, including the original GPT-2 vocabulary and the newly added special tokens. Each text sample is mapped to a sequence of token IDs in $\{0, \dots, |\mathcal{V}| - 1\}$.

For the final inputs, we truncate or pad every sequence to a fixed length L_{\max} . Thus each text sample is represented as

$$x = (x_1, \dots, x_{L_{\max}}), \quad x_\ell \in \{0, \dots, |\mathcal{V}| - 1\}.$$

Texts longer than L_{\max} tokens are truncated, and texts shorter than L_{\max} tokens are padded on the right with $\langle \text{pad} \rangle$. Together with the token IDs, we store an attention mask

$$a = (a_1, \dots, a_{L_{\max}}), \quad a_\ell \in \{0, 1\},$$

where $a_\ell = 1$ indicates a valid token position and $a_\ell = 0$ indicates a padding position. Hence, after tokenization, each sample is represented by

$$(x, a) \in \{0, \dots, |\mathcal{V}| - 1\}^{L_{\max}} \times \{0, 1\}^{L_{\max}}.$$

The model is trained only on the tokenized normal examples from the training split, while the full tokenized test split is used for evaluation. The same tokenizer and maximum sequence length are used for both training and testing.

B.2 Evaluation Criteria

We evaluate anomaly detection performance using ROC-AUC and PR-AUC. For each test sample \mathbf{x}_i , let $y_i \in \{0, 1\}$ denote its ground-truth label, where $y_i = 0$ indicates a normal sample and $y_i = 1$ indicates an anomalous sample. Each method produces an anomaly score $S(\mathbf{x}_i)$, where a larger score indicates stronger evidence of anomaly.

ROC-AUC measures the global ranking quality between anomalous and normal samples. Equivalently, it can be interpreted as the probability that a randomly chosen anomalous sample receives a higher score than a randomly chosen normal sample:

$$\text{AUC}_{\text{ROC}} = \mathbb{P}(S(\mathbf{x}^+) > S(\mathbf{x}^-)),$$

where \mathbf{x}^+ denotes a randomly selected anomalous sample and \mathbf{x}^- denotes a randomly selected normal sample.

PR-AUC summarizes the precision–recall tradeoff obtained by thresholding the anomaly scores. For a threshold γ , samples with $S(\mathbf{x}_i) \geq \gamma$ are predicted as anomalies, and

$$\text{Precision}(\gamma) = \frac{\text{TP}(\gamma)}{\text{TP}(\gamma) + \text{FP}(\gamma)}, \quad \text{Recall}(\gamma) = \frac{\text{TP}(\gamma)}{\text{TP}(\gamma) + \text{FN}(\gamma)}.$$

We report PR-AUC as average precision, which corresponds to a step-wise area under the precision–recall curve.

B.3 MaskDiff-AD Hyperparameters

For all variants of MaskDiff-AD, we use fixed hyperparameters across datasets rather than validation-based or per-dataset tuning. We adopt the standard linear absorbing schedule $\alpha_t = 1 - t$, so a probe level τ_ℓ has mask probability $1 - \alpha_{\tau_\ell} = \tau_\ell$. All reconstruction scores are averaged over the specified probe levels and independently generated masked probe views.

The parametric tabular model uses the uniform probe grid $\tau_\ell \in \{0.1, 0.2, \dots, 0.9\}$ and 16 masked probe views per probe level. Its reconstruction network uses embedding dimension 256, hidden dimension 512, three MLP layers, and dropout 0.1. The model is trained for 20 epochs with AdamW using learning rate 10^{-3} and weight decay 10^{-5} .

The non-parametric tabular model uses the probe grid $\tau_\ell \in \{0.15, 0.30, 0.45, 0.60\}$ and 8 masked probe views per probe level. It has no trainable neural parameters and takes all normal training samples as the reference set. Masked-coordinate reconstruction probabilities are estimated using

the visible-coordinate Hamming kernel $K_\lambda(\tilde{\mathbf{x}}, \mathbf{x}^{(n)}) = \exp\{-\lambda d_{\text{vis}}(\tilde{\mathbf{x}}, \mathbf{x}^{(n)})\}$ with bandwidth $\lambda = 1$, where d_{vis} denotes the Hamming distance restricted to visible coordinates.

For text experiments, we use the GPT-2 tokenizer only, without using the pretrained GPT-2 language model or pretrained GPT-2 token embeddings. The text model uses the same uniform probe grid as the parametric tabular model, $\tau_\ell \in \{0.1, 0.2, \dots, 0.9\}$, and 24 masked probe views per probe level. The reconstruction model is an 8-layer Transformer encoder with hidden dimension 512, 16 attention heads, feed-forward dimension 2048, and dropout 0.1. It is trained for 20 epochs with AdamW using learning rate 10^{-3} and weight decay 10^{-5} .

B.4 Baselines

We compare against classical anomaly detection baselines, DTE-based variants, and recent tabular or text anomaly detection methods. All baselines are evaluated under the same normal-only setting: each method is fitted only on normal training samples, and anomaly labels are used only for test-time evaluation.

Hyperparameter setup. We use a fixed default hyperparameter configuration across datasets and random seeds, rather than performing per-dataset hyperparameter search. The main settings for all tabular baselines are summarized in Table 4.

Tabular baselines. For categorical and mixed-type tabular datasets, categorical features are encoded as discrete symbols. Numerical features are discretized by quantile binning using only the normal training subset. By default, we use 10 quantile bins, treat numerical features with at most 20 distinct values as discrete features, and use an explicit unknown bucket for unseen categories. The fitted preprocessing parameters are then reused for the test set.

Hamming- k NN, ECOD, and COPOD are applied to the ordinal/binning representation. For methods whose behavior may be affected by artificial ordering of category IDs, including Isolation Forest and neural tabular baselines, we use the one-hot representation. DTE variants are also run on the one-hot representation of the discretized features, so that they use the same discretized information as the other baselines.

Text baselines. For text anomaly detection, we use datasets from NLP-ADBench [12] and compare against the baseline results reported in that benchmark. NLP-ADBench evaluates 19 text anomaly detection baselines, including end-to-end methods such as DATE [46] and FATE [47], as well as embedding-based methods. For the embedding-based baselines, BERT embeddings [48] and OpenAI text embeddings [49] are used as fixed document representations, followed by LOF [50], DeepSVDD [44], ECOD [24], Isolation Forest [23], SO-GAAL [51], AE [52], VAE [53], and LUNAR [54]. We evaluate our method on the same datasets and report ROC-AUC and PR-AUC using the same evaluation convention.

B.5 Sensitivity Analysis

Figure 4 provides additional sensitivity results on U2R and Bank. Compared with the Vehicle Claims result in Figure 3, these datasets exhibit different best-performing single probe levels. This supports our choice of using a fixed multi-probe score that aggregates over a uniform probe grid, rather than tuning the probe level separately for each dataset. In low-view regimes, the average masked reconstruction loss in Eq. (8) is occasionally marginally better than the original masked

Table 4: Default hyperparameters for tabular baselines. The same settings are used across datasets and seeds.

Method	Input	Main settings
COPOD	ordinal/binned	PyOD default
DeepSVDD	one-hot	100 epochs, batch size 64, learning rate 10^{-3} , hidden dims 100, 50
DRL	one-hot	200 epochs, batch size 512, learning rate 0.05, LR decay 0.98
DTE-Categorical / InvGamma / Gaussian	one-hot	100 epochs, batch size 128, learning rate 10^{-4} , MLP hidden dims 256, 512, 256
ECOD	ordinal/binned	PyOD default
GOAD	one-hot	100 epochs, batch size 64, learning rate 10^{-3} , 256 transformations
Hamming- k NN	ordinal/binned	$k = 25$, Hamming distance
ICL	one-hot	100 epochs, batch size 64, learning rate 10^{-3} , hidden dims 100, 50
IForest	one-hot	300 trees, <code>max_samples=auto</code> , <code>contamination=auto</code>
MCM	one-hot	200 epochs, batch size 512, learning rate 0.05, LR decay 0.98

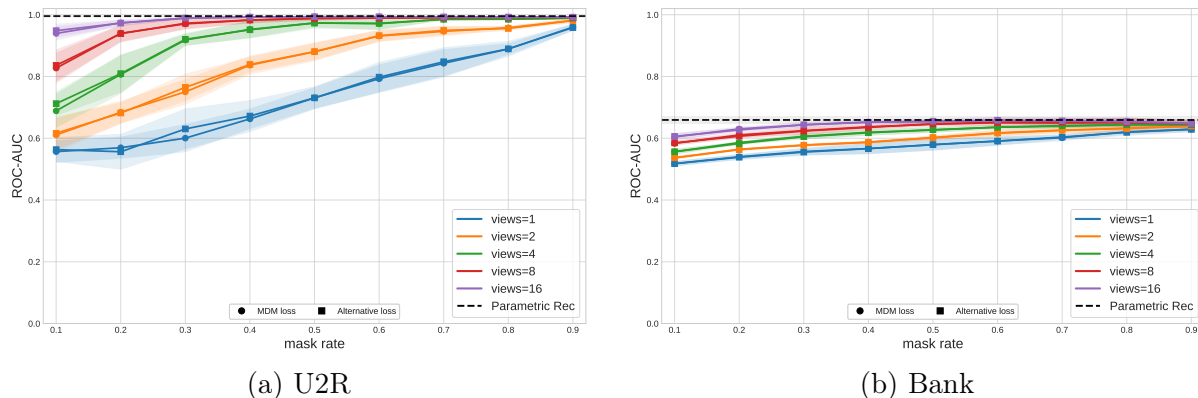


Figure 4: Additional sensitivity analysis of Parametric MaskDiff-AD to the probe mask rate τ on U2R and Bank. Together with the Vehicle Claims result in Figure 3, these results show that the optimal single probe level can vary across datasets, motivating the fixed multi-probe aggregation used in the main experiments.

diffusion loss on some datasets, possibly because it is more closely aligned with the normalized test-time reconstruction score.

B.6 Runtime and Comparison

We report runtime in Table 5. The comparison is conducted on two tabular datasets with different scales: Bank contains 41,188 samples with 10 features, while Vehicle Claims contains 268,255 samples with 18 features. Runtime is decomposed into training or fitting time, inference time, and total time.

The results show that Parametric MaskDiff-AD achieves a favorable balance between training cost and inference efficiency. On the large Vehicle Claims dataset, Parametric MaskDiff-AD takes 31.64 seconds for training and 16.28 seconds for inference, leading to a total runtime of 47.92 seconds. This is substantially faster than several deep baselines such as GOAD, ICL, and MCM, while also avoiding the high test-time cost of Non-parametric MaskDiff-AD. On the Bank dataset, Parametric MaskDiff-AD remains efficient, with a total runtime of 5.71 seconds.

The comparison also highlights the different computational profiles of the two MaskDiff-AD variants. Non-parametric MaskDiff-AD does not require model training, but its test-time cost can become large because each test sample is compared against the normal training set through masked-view reconstruction. This effect is especially clear on Vehicle Claims, where its inference time reaches 3005.69 seconds. In contrast, Parametric MaskDiff-AD amortizes the reconstruction model

Table 5: Runtime comparison on the Bank and Vehicle Claims datasets.

Method	Bank			Vehicle Claims		
	Train / Fit	Inference	Total	Train / Fit	Inference	Total
Parametric MaskDiff-AD	3.87	1.84	5.71	31.64	16.28	47.92
Non-parametric MaskDiff-AD	0.00	4.81	4.81	0.00	3005.69	3005.69
COPOD	0.01	0.02	0.03	0.13	0.22	0.35
DeepSVDD	18.73	0.03	18.75	130.88	0.20	131.09
DRL	20.24	0.02	20.25	132.68	0.12	132.80
DTE-Categorical	17.21	0.02	17.23	138.35	0.25	138.59
DTE-Gaussian	15.33	0.02	15.35	130.23	0.24	130.47
DTE-InvGamma	18.03	0.03	18.05	144.01	0.25	144.27
ECOD	0.12	0.02	0.14	0.24	0.25	0.49
GOAD	122.88	1.40	124.27	768.66	22.35	791.02
Hamming-kNN	0.00	3.17	3.17	0.00	65.66	65.66
ICL	61.86	0.11	61.97	817.37	2.02	819.39
IForest	0.25	0.09	0.35	0.35	1.35	1.70
MCM	49.69	0.04	49.72	678.01	0.63	678.64

during training and then performs inference through a neural network, making it more scalable on larger datasets. For smaller or medium-scale datasets such as Bank, the non-parametric variant is still feasible, but the parametric version provides a more consistent runtime profile across dataset sizes.

C Proofs of Theoretical Guarantee

Proof of Theorem 1. Recall the definitions for S^* and S_{rec}^* in Eqs. (9) and (10), respectively. With these, we also have

$$\Delta_{\text{KL}}(\mathbf{x}) = S_{\text{rec}}^*(\mathbf{x}) - S^*(\mathbf{x}) = \frac{1}{L} \sum_{\ell=1}^L \mathbb{E}_{\tilde{\mathbf{x}} \sim q_{\tau_\ell}(\cdot|\mathbf{x})} \left[\frac{\sum_{j \in M(\tilde{\mathbf{x}})} \log \frac{q^j(x_j|\tilde{\mathbf{x}}, \tau_\ell)}{p_\theta^j(x_j|\tilde{\mathbf{x}}, \tau_\ell)}}{|M(\tilde{\mathbf{x}})| \vee 1} \right]. \quad (11)$$

When the log-likelihoods are bounded, we have that

$$|S_{\text{rec}}(\mathbf{x})| \leq C, \quad |S_{\text{rec}}^*(\mathbf{x})| \leq C, \quad |S^*(\mathbf{x})| \leq C, \quad |\Delta_{\text{KL}}(\mathbf{x})| \leq 2C.$$

As follows, we provide the proofs for the Type-I error and the Type-II error, respectively.

Type-I error Note that

$$S_{\text{rec}}(\mathbf{x}) = \underbrace{S_{\text{rec}}(\mathbf{x}) - S_{\text{rec}}^*(\mathbf{x})}_{\text{stochastic test-time error from finite number of views}} + \underbrace{S_{\text{rec}}^*(\mathbf{x}) - S^*(\mathbf{x})}_{\text{training error from imperfect model}} + S^*(\mathbf{x}).$$

So, we have

$$\begin{aligned}
& \mathbb{P}_{\mathbf{x} \sim q_0}(S_{\text{rec}}(\mathbf{x}) \geq \gamma) \\
&= \mathbb{P}_{\mathbf{x} \sim q_0}((S_{\text{rec}}(\mathbf{x}) - S_{\text{rec}}^*(\mathbf{x})) + (S_{\text{rec}}^*(\mathbf{x}) - S^*(\mathbf{x}) - \epsilon) + (S^*(\mathbf{x}) - \mu_0^*) \geq \gamma - \mu_0^* - \epsilon) \\
&\stackrel{(i)}{\leq} \mathbb{P}_{\mathbf{x} \sim q_0}\left(S_{\text{rec}}(\mathbf{x}) - S_{\text{rec}}^*(\mathbf{x}) \geq \frac{\gamma - \mu_0^* - \epsilon}{3}\right) + \mathbb{P}_{\mathbf{x} \sim q_0}\left(\Delta_{KL}(\mathbf{x}) - \mathbb{E}_{\mathbf{x} \sim q_0}[\Delta_{KL}(\mathbf{x})] \geq \frac{\gamma - \mu_0^* - \epsilon}{3}\right) \\
&\quad + \mathbb{P}_{\mathbf{x} \sim q_0}\left(S^*(\mathbf{x}) - \mu_0^* \geq \frac{\gamma - \mu_0^* - \epsilon}{3}\right) \\
&\stackrel{(ii)}{\leq} \exp\left(-\frac{2Kt^2}{C^2}\right) + \exp\left(-\frac{Lt^2}{2C^2}\right) + \exp\left(-\frac{2Lt^2}{C^2}\right),
\end{aligned}$$

where $t := (\gamma - \mu_0^* - \epsilon)/3$, (i) follows from the union bound that

$$\mathbb{P}\left(\sum_{i=1}^3 U_i \geq u\right) \leq \sum_{i=1}^3 \mathbb{P}(U_i \geq u/3),$$

and (ii) follows from Hoeffding's inequality.

Type-II error The analysis is similar. When there is no estimation error, we have $S_{\text{rec}}^* = S^*$, and thus

$$S_{\text{rec}}(\mathbf{x}) = S_{\text{rec}}(\mathbf{x}) - S_{\text{rec}}^*(\mathbf{x}) + S^*(\mathbf{x}).$$

So, we have

$$\begin{aligned}
& \mathbb{P}_{q'}(S_{\text{rec}}(\mathbf{x}) < \gamma) \\
&= \mathbb{P}_{q'}((S_{\text{rec}}(\mathbf{x}) - S_{\text{rec}}^*(\mathbf{x})) + (S^*(\mathbf{x}) - \mu_1^*) < \gamma - \mu_1^*) \\
&\stackrel{(iii)}{\leq} \mathbb{P}_{q'}\left(S_{\text{rec}}(\mathbf{x}) - S_{\text{rec}}^*(\mathbf{x}) < \frac{\gamma - \mu_1^*}{2}\right) + \mathbb{P}_{q'}\left(S^*(\mathbf{x}) - \mu_1^* < \frac{\gamma - \mu_1^*}{2}\right) \\
&\stackrel{(iv)}{\leq} \exp\left(-\frac{K(\mu_1^* - \gamma)^2}{2C^2}\right) + \exp\left(-\frac{L(\mu_1^* - \gamma)^2}{2C^2}\right),
\end{aligned}$$

where (iii) holds again by union bound:

$$\mathbb{P}(U_1 + U_2 \leq -u) \leq \sum_{i=1}^2 \mathbb{P}(U_i \leq -u/2),$$

and (iv) holds again by Hoeffding's inequality. □

Table 6: ROC-AUC on tabular datasets over five random seeds.

Method	ad	ad362	apas	bank	chess	cmc	covertype	probe	r10	solar	u2r	vehicle_claims	w7a
Parametric MaskDiff-AD	78.86 (2.34)	67.93 (4.78)	83.15 (3.36)	65.90 (0.91)	73.55 (7.74)	59.30 (8.97)	91.92 (0.68)	98.42 (0.69)	99.14 (0.14)	86.00 (4.61)	99.55 (0.10)	96.38 (0.09)	62.53 (1.93)
Non-parametric MaskDiff-AD	93.43 (1.72)	64.69 (4.78)	80.01 (1.85)	63.68 (0.89)	55.96 (11.17)	56.85 (11.64)	95.47 (0.21)	98.38 (0.69)	99.09 (0.12)	85.85 (3.48)	99.11 (0.12)	85.14 (0.15)	65.05 (1.44)
COPOD	73.85 (2.05)	65.12 (4.77)	64.15 (3.96)	59.31 (2.19)	70.76 (27.06)	51.07 (10.94)	97.72 (0.68)	98.33 (0.68)	98.83 (0.13)	87.04 (5.04)	97.74 (0.67)	67.18 (0.27)	58.68 (1.49)
DeepSVDD	74.09 (12.18)	59.93 (12.83)	57.45 (17.36)	52.09 (2.73)	45.68 (10.43)	62.17 (5.69)	47.84 (29.21)	83.32 (4.83)	96.88 (3.31)	81.76 (3.82)	76.77 (24.13)	77.41 (1.46)	81.23 (3.32)
DTE-Categorical	85.18 (2.50)	86.37 (2.95)	86.37 (2.95)	98.06 (1.06)	61.17 (0.76)	65.20 (6.77)	94.21 (1.06)	97.88 (0.26)	98.31 (0.16)	78.06 (9.31)	99.01 (0.15)	69.52 (0.30)	81.36 (1.10)
DTE-InvGamma	81.25 (1.71)	86.57 (1.91)	86.57 (1.91)	86.57 (1.91)	61.34 (0.66)	65.20 (6.77)	94.21 (1.06)	97.88 (0.26)	98.31 (0.16)	78.06 (9.31)	99.01 (0.15)	69.52 (0.30)	81.36 (1.10)
DTE-Gaussian	91.27 (1.19)	66.57 (5.60)	72.40 (2.83)	62.52 (0.96)	61.34 (3.37)	57.71 (12.17)	64.68 (15.46)	98.15 (0.10)	99.32 (0.11)	82.84 (4.87)	99.61 (0.07)	84.65 (0.54)	84.13 (2.55)
DRL	79.95 (1.49)	65.59 (6.70)	73.87 (6.00)	58.72 (2.98)	45.64 (13.10)	61.60 (8.43)	44.53 (16.41)	98.85 (0.24)	99.09 (0.48)	82.13 (5.89)	97.04 (3.18)	68.31 (5.31)	64.01 (12.23)
GOAD	73.92 (2.08)	65.59 (4.63)	67.21 (3.51)	60.90 (1.67)	62.89 (2.28)	54.13 (9.53)	97.82 (0.07)	98.35 (0.10)	98.83 (0.13)	85.78 (4.44)	97.53 (1.38)	66.86 (0.51)	59.13 (1.48)
ECOD	74.72 (2.42)	65.00 (4.48)	65.10 (4.91)	57.06 (1.25)	62.26 (12.66)	53.27 (9.48)	95.43 (0.82)	98.39 (0.10)	98.72 (0.14)	87.06 (3.97)	98.96 (0.12)	58.04 (0.96)	50.03 (1.84)
Hamming-kNN	80.97 (2.02)	71.69 (3.49)	86.89 (1.90)	64.50 (0.77)	93.22 (1.87)	60.59 (9.43)	50.00 (0.00)	89.17 (0.77)	98.90 (0.12)	83.67 (5.76)	87.87 (1.33)	72.98 (0.19)	52.36 (1.35)
ICL	79.69 (4.19)	60.49 (3.52)	44.57 (18.25)	60.81 (2.53)	65.53 (1.94)	57.17 (18.61)	36.11 (21.32)	23.85 (7.33)	98.70 (0.27)	82.43 (9.17)	28.50 (31.30)	81.43 (2.65)	76.58 (2.93)
IForest	42.17 (1.58)	66.49 (4.75)	52.75 (1.09)	57.49 (0.94)	59.32 (1.80)	68.19 (14.57)	93.83 (2.45)	96.67 (0.26)	96.90 (0.51)	83.16 (5.45)	96.69 (0.85)	46.15 (1.71)	41.26 (4.69)
MCM	75.47 (5.24)	63.45 (5.47)	67.51 (3.48)	60.75 (1.94)	56.75 (22.41)	55.85 (12.21)	91.43 (5.43)	95.78 (5.30)	98.61 (0.20)	64.54 (19.06)	95.65 (5.55)	69.75 (2.51)	54.05 (5.72)

Table 7: PR-AUC on tabular datasets over five random seeds.

Method	ad	ad362	apas	bank	chess	cmc	covertype	probe	r10	solar	u2r	vehicle_claims	w7a
Parametric MaskDiff-AD	64.40 (3.96)	3.76 (0.94)	4.91 (1.17)	23.90 (1.19)	0.69 (0.48)	5.89 (3.37)	5.50 (0.83)	91.59 (0.68)	70.34 (3.75)	20.29 (6.55)	46.37 (6.45)	93.04 (0.06)	13.71 (2.47)
Non-parametric MaskDiff-AD	86.82 (3.80)	4.02 (0.88)	2.46 (0.44)	21.39 (0.83)	0.29 (0.30)	5.45 (4.98)	9.69 (0.80)	89.88 (0.34)	69.03 (3.78)	17.48 (4.24)	34.60 (4.06)	71.39 (0.28)	15.54 (2.56)
COPOD	56.18 (4.18)	2.83 (0.37)	2.46 (0.44)	13.82 (1.67)	0.68 (0.82)	3.95 (2.19)	12.84 (0.47)	82.92 (0.67)	60.20 (4.51)	21.89 (6.23)	35.63 (12.34)	38.89 (0.42)	4.66 (0.40)
DeepSVDD	52.23 (17.63)	2.61 (1.23)	2.63 (1.67)	13.84 (0.83)	0.10 (0.03)	5.11 (1.89)	1.57 (1.12)	74.61 (4.29)	68.71 (5.30)	22.14 (5.65)	33.54 (18.24)	71.22 (1.15)	55.84 (7.10)
DTE-Categorical	59.87 (7.51)	3.24 (0.28)	5.11 (1.09)	27.71 (1.74)	0.15 (0.10)	3.83 (0.61)	4.98 (0.25)	73.54 (2.60)	52.03 (4.20)	22.83 (2.66)	22.83 (2.66)	34.93 (0.27)	40.88 (4.20)
DTE-InvGamma	55.73 (15.85)	3.24 (0.28)	5.56 (2.33)	18.83 (3.44)	0.14 (0.04)	3.19 (0.67)	6.04 (2.39)	79.05 (6.78)	30.92 (9.94)	19.15 (8.40)	41.56 (29.44)	82.69 (1.46)	52.83 (3.56)
DTE-Gaussian	81.42 (2.97)	5.07 (2.18)	4.38 (1.07)	19.81 (1.39)	0.18 (0.07)	3.68 (1.61)	2.51 (0.90)	91.86 (0.52)	66.04 (5.54)	21.82 (8.78)	71.36 (3.45)	72.39 (0.93)	45.98 (3.46)
DRL	53.25 (5.60)	3.58 (1.22)	3.24 (1.23)	16.11 (1.73)	0.10 (0.05)	6.42 (3.07)	1.36 (1.92)	92.07 (0.57)	66.69 (12.28)	21.93 (7.59)	57.29 (15.54)	53.97 (8.83)	24.22 (14.89)
ECOD	56.29 (4.17)	2.85 (0.37)	2.63 (0.42)	19.16 (2.18)	0.28 (0.21)	3.82 (1.89)	13.00 (0.47)	83.03 (1.61)	60.22 (4.51)	21.85 (5.43)	33.75 (15.29)	38.53 (0.61)	4.77 (0.41)
GOAD	54.98 (4.92)	2.72 (0.35)	2.62 (0.68)	15.40 (1.06)	0.30 (0.28)	6.98 (8.48)	10.21 (2.13)	90.09 (1.05)	56.83 (3.89)	21.23 (6.15)	47.75 (12.90)	26.84 (0.68)	2.96 (0.17)
Hamming-kNN	65.64 (3.75)	3.48 (0.57)	3.48 (0.57)	21.16 (0.88)	0.47 (0.00)	5.99 (5.52)	0.47 (0.00)	78.90 (1.40)	59.61 (4.34)	17.87 (5.56)	60.29 (4.39)	46.22 (0.32)	3.07 (0.17)
ICL	58.13 (6.48)	3.32 (0.80)	1.33 (0.50)	20.19 (3.51)	0.37 (0.38)	4.26 (3.15)	1.08 (0.65)	21.48 (7.94)	61.78 (3.56)	19.85 (8.81)	22.91 (30.33)	74.25 (2.89)	33.82 (3.66)
IForest	11.16 (0.27)	3.02 (0.56)	1.58 (0.12)	15.23 (0.49)	7.03 (0.53)	7.03 (0.53)	5.39 (2.15)	67.72 (2.37)	39.91 (5.05)	18.50 (3.90)	19.14 (1.90)	19.47 (0.75)	2.32 (0.68)
MCM	47.72 (9.38)	2.63 (0.61)	2.31 (0.55)	19.20 (2.98)	10.14 (0.24)	1.80 (3.27)	6.88 (2.34)	85.97 (4.36)	36.23 (7.25)	14.25 (11.34)	42.34 (22.82)	41.25 (3.46)	7.10 (2.24)